MARSHALL

34 P.

NASA Contractor Report 3990

IN-11108

Pof
Pub
[illegible]
H

Turbulent Flow Field Predictions in Sharply Curved Turn-Around Ducts

ND 776801

L. Michael Santi

GRANT NGT-01-008-021
JUNE 1986

NASA

NASA Contractor Report 3990

Turbulent Flow Field Predictions in Sharply Curved Turn-Around Ducts

L. Michael Santi
Memphis State University
Memphis, Tennessee

Prepared for
George C. Marshall Space Flight Center
under Grant NGT-01-008-021

National Aeronautics
and Space Administration

**Scientific and Technical
Information Branch**

1986

TABLE OF CONTENTS

LIST OF ILLUSTRATIONS

LIST OF ILLUSTRATIONS (Concluded)

NOMENCLATURE

Symbol	Definition
$C_{\mu 0}$	constant (=0.09) in traditional k-ε model turbulent viscosity expression
C_μ	spatially variant function in modified k-ε model turbulent viscosity expression ($\mu_t = C_\mu \rho k^2/\varepsilon$)
C_w	constant in wall function correction ($=\kappa/C_{\mu 0}^{3/4}$), see equation (13)
D	duct width
D_{ij}	dissipation term in the Reynolds stress transport equations
E	east side cell, see Figure 12
F	cubic polynomial in $\sqrt{C_\mu}$, see equation (12)
k	turbulent kinetic energy
ℓ	turbulence length scale
ℓ_o	turbulent length scale for flow over a plane
N	north side cell, see Figure 12
P	time averaged pressure
P_d	turbulent energy production rate
P_e	exit plane pressure assumed uniform
P_{ij}	production term in the Reynolds stress transport equations
r	radial direction coordinate
r_i	duct inner convex wall radius of curvature
r_o	duct outer concave wall radius of curvature
R_c	duct centerline radius of curvature ($=[r_i+r_o]/2$)
S	south side cell, see Figure 12
S_r, S_θ	momentum source terms, see equations (5) and (6)
$\overline{u_r u_\theta}$, $\overline{u_r^2}$, $\overline{u_\theta^2}$	Reynolds stress components in cylindrical coordinates
U	time averaged streamwise velocity

Symbol	Definition
$\bar{U}$	cross-stream averaged streamwise velocity
U_r, U_θ	time averaged velocity components in cylindrical coordinates
W	west side cell, see Figure 12
y	distance from the duct inner convex surface measured in the radial direction
β	empirical constant in curvature modified length scale, see equation (1)
ε	energy dissipation rate
ε_{ij}	dissipation term in the Reynolds stress transport equations
κ	von Karman constant
μ	absolute viscosity
μ_t	turbulent viscosity
μ_{eff}	effective viscosity ($=\mu_t+\mu$)
Π_{ij}	pressure strain term in the Reynolds stress transport equations
ρ	mass density
θ	angular position measured from the duct entrance plane
BFC	body-fitted coordinates
FDP	fully developed pipe or duct
SSME	Space Shuttle Main Engine
TAD	turn around duct

CONTRACTOR REPORT

TURBULENT FLOW FIELD PREDICTIONS IN SHARPLY CURVED TURN AROUND DUCTS

INTRODUCTION

Performance demands of modern machinery require designs exhibiting both dimensional and operational economy. In applications which require the motion of a working fluid, these economic considerations have fueled a proliferation of devices containing complex flow passages through which fluids travel at extreme rates. Examples include flows in turbomachinery, nozzles, diffusers, and curved ducts. Of primary interest in this investigation are flows in sharply curved turn around ducts (TAD's) common in rocket engine design, including current and projected versions of the Space Shuttle Main Engine (SSME).

Despite the design impetus provided by increased performance requirements, a detailed understanding of turbulent fluid motion with significant streamline curvature is inhibited by formidable obstacles to both experimental measurement and computational study. Since the system of motion governing equations for turbulent flows is essentially incomplete, advances in the computational prediction of turbulent field characteristics are tied to turbulence models requiring a sound empirical basis. In the case of sharply curved passages and extreme flow rates prevalent in modern equipment, the experimental basis required for detailed flow prediction is difficult to obtain with confidence.

An example of a high rate, strongly curved flow field with little experimental basis on which to develop adequate turbulence models occurs in the SSME fuel side turbopump TAD. A simplified two-dimensional version of this TAD configuration is depicted in Figure 1. Although several studies of turbulent curved duct flow have been reported [1-7], none deals with curvatures or rates of the magnitude occurring in the SSME. The state of turbulence modeling in general is such that little confidence can be placed in extrapolation of the results of these investigations to a broader class of curved flows.

The sensitivity of turbulent flow characteristics to even mild streamline curvatures has been discussed by Bradshaw [8]. In this extensive review, a curvature modified length scale of the form

$$\ell = \left(1 \pm \beta \frac{U_\theta/r}{U_{\theta,r}}\right) \ell_o \qquad (1)$$

was proposed. In this relation β is an empirical constant of order 10, ℓ_o is a length scale appropriate for plane flow, and subscripts following a comma indicate differentiation with respect to the specified variable (e.g., $U_{\theta,r} = \partial U_\theta / \partial r$). Inclusion of this curvature modified scale into a general mixing length model of turbulent motion is hampered by the flow dependence of both β and ℓ_o. Lack of extensive applicability is characteristic of all mixing length modeling strategies.

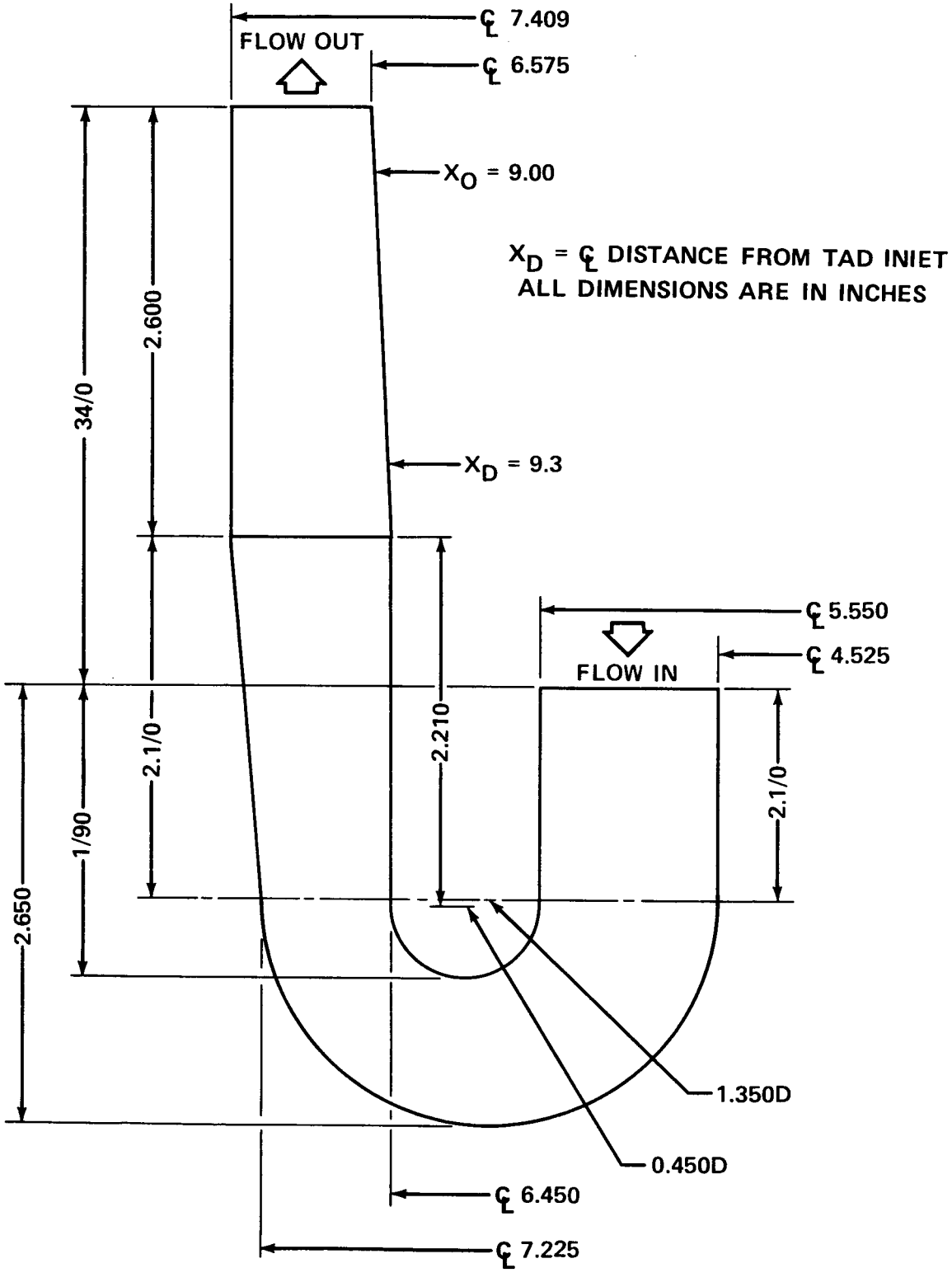

Figure 1. Early SSME fuel side turbopump TAD design.

Launder et al. [4] have proposed a two-equation closure model with the length scale dependence obtained from solution of the equations for turbulent kinetic energy and the energy dissipation rate. The direct effect of curvature is introduced as a single term in the dissipation equation which is proportional to the turbulent Richardson number. The required proportionality constant appears as a new empiricism.

Recently, an extended k-ε turbulence model, which uses algebraic approximations for the Reynolds stress transport equations in order to develop an explicit curvature dependent expression for C_μ in $\nu_t = C_\mu k^2/\varepsilon$, has been reported by Pourahmadi and Humphrey [9,10] and applied to curved duct flows. The new expression for C_μ accounts simultaneously for effects of streamline curvature and pressure strain with wall dampening. The development is a formidable task, calling upon a variety of traditional turbulence modeling approximations [11-15]. The approach taken by Pourahmadi and Humphrey presents a promising explicit curvature model with roots, albeit approximate, in the Reynolds stress transport equations. Unfortunately, previous results based on this computational procedure appear to be based on a rather fundamental algebraic error which will be addressed in subsequent sections of this report.

Another approach which has been pursued is to include curvature effects in a modified wall law [3,16]. This method is well suited for near wall treatment in coarse grid numerical calculations of turbulent boundary layers under adverse pressure gradients. Incorporation into computational procedures involving strongly curved, fully elliptic flow fields is certainly plausible.

Because of the scarcity of reliable experimental data involving high rate flows in sharply curved passages, and the difficulty in extrapolating turbulent model predictions, none of the above described curvature modified turbulence models can be objectively recommended. Each, however, presents an opportunity for computational investigation, refinement, and comparison with results of standard turbulence models as well as experimentation.

OBJECTIVES

The objectives of this investigation have a dual character. On one hand, computational predictions of turbulent flow properties in sharply curved TAD's are sought in order to provide additional information on the operational characteristics of devices incorporating such flows. Of specific interest are TAD flows in the SSME fuel side turbopump. As such, results of this investigation fall into the category of computational analysis. A second view is more appropriate, however, with results of the investigation taken as presenting contributions to the base of computational experimentation needed to improve general models of turbulent flow with significant streamline curvature. The data base building aspect of this study is considered to be the primary goal.

In order to achieve this primary goal, three specific objectives were established.

1) To estimate the general characteristics of turbulent flows in sharply curved TAD's using a standard k-ε turbulence model on an abbreviated geometry as displayed in Figure 2.

2) To implement and test a specific turbulence model which explicitly incorporates the effects of streamline curvature and pressure strain.

3) To examine the elliptic character of the governing motion equations by implementing an orthogonal, body-fitted coordinate reference frame analysis on an extended duct geometry shown in Figure 3.

Background information concerning each of the three stated objectives is provided in the following section of this report.

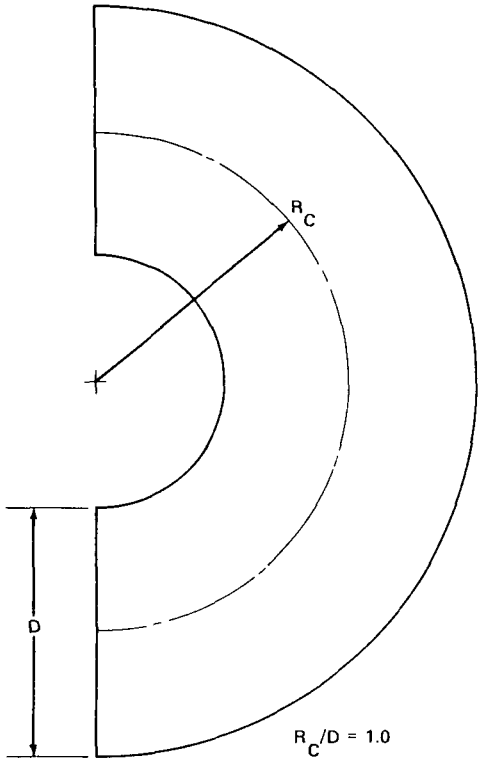

Figure 2. Simple TAD analysis geometry.

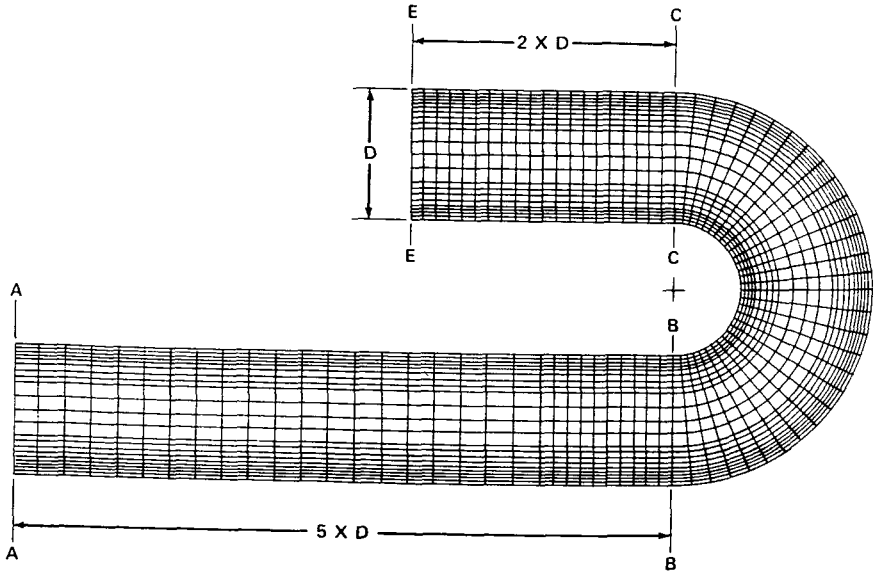

Figure 3. Geometry and grid pattern for BFC TAD analyses: 20 x 80 grid.

BACKGROUND INFORMATION

Equations governing the motion of steady, two-dimensional, turbulent flow of an incompressible, Newtonian fluid in cylindrical coordinates are given below [10].

Continuity:

$$U_{r,r} + U_{\theta,\theta}/r + U_r/r = 0 \tag{2}$$

r-Momentum:

$$\rho[U_r U_{r,r} + U_\theta U_{r,\theta}/r - U_\theta^2/r] = -P_{,r} + (\mu_{eff} r U_{r,r})_{,r}/r + (\mu_{eff} U_{r,\theta}/r)_{,\theta}/r$$
$$-\mu_{eff} U_r/r^2 - 2\mu_{eff} U_{\theta,\theta}/r^2 + S_r \tag{3}$$

θ-Momentum:

$$\rho[U_r U_{\theta,r} + U_\theta U_{\theta,\theta}/r + U_r U_\theta/r] = -P_{,\theta}/r + (\mu_{eff} r U_{\theta,r})_{,r}/r + (\mu_{eff} U_{\theta,\theta}/r)_{,\theta}/r$$
$$- \mu_{eff} U_\theta/r^2 + 2\mu_{eff} U_{r,\theta}/r^2 + S_\theta \tag{4}$$

In equations (3) and (4) above, the Boussinesq assumption has been employed to model the Reynolds stresses in terms of mean velocity gradients and a turbulent viscosity component. The momentum source terms S_r and S_θ are given by the relations below.

$$S_r = [\mu_t r(U_\theta/r)_{,r}]_{,\theta}/r + (\mu_t r U_{r,r})_{,r}/r - \mu_t U_r/r^2 \tag{5}$$

$$S_\theta = [\mu_t(2U_r/r + U_{\theta,\theta}/r)]_{,\theta}/r + [\mu_t(U_{r,\theta} - U_\theta)/r]_{,r} + \mu_t(U_{\theta,r} - U_\theta/r)/r \tag{6}$$

In order to provide and solve for spatial variation of the turbulent viscosity μ_t, the k-ε turbulence model as described by Launder and Spalding [17] was employed. This two equation model has been compared favorably to a variety of turbulence modeling schemes [18]. It has been tested on a wide range of flow configurations, exhibiting some degree of universality with an acceptable degree of complexity. Following this approach, μ_t is determined by the relation

$$\mu_t = C_\mu \rho k^2/\varepsilon \quad , \tag{7}$$

where the turbulent kinetic energy and dissipation rate are determined upon solving the differential transport equations given below [10,19].

Turbulent kinetic energy k:

$$\rho[U_r k_{,r} + U_\theta k_{,\theta}/r] = (\mu_{eff} r k_{,r}/\sigma_k)_{,r}/r + (\mu_{eff} k_{,\theta}/\sigma_k)_{,\theta}/r^2 - \rho\varepsilon + P_d \qquad (8)$$

Energy dissipation rate ε:

$$\rho[U_r \varepsilon_{,r} + U_\theta \varepsilon_{,\theta}/r] = (\mu_{eff} r \varepsilon_{,r}/\sigma_\varepsilon)_{,r}/r + (\mu_{eff} \varepsilon_{,\theta}/\sigma_\varepsilon)_{,\theta}/r^2 + C_{\varepsilon 1} \varepsilon P_d/k$$

$$- C_{\varepsilon 2} \rho \varepsilon^2/k \qquad (9)$$

The production term P_d in equations (8) and (9) is given by the relation

$$P_d = \mu_t\{2[(U_{r,r})^2 + (U_{\theta,\theta}/r)^2 - U_\theta(U_{r,\theta}/r + U_{\theta,r})/r + U_r(U_r + 2U_{\theta,\theta})/r^2$$

$$+ U_{r,\theta}U_{\theta,r}/r] + (U_\theta/r)^2 + (U_{\theta,r})^2 + (U_{r,\theta}/r)^2\} \quad . \qquad (10)$$

The numerical procedure used to solve the discretized form of equations (2), (3), (4), (8) and (9) was provided by the proprietary PHOENICS computer code supplied and supported by CHAM of North America. A discussion of the philosophical and mathematical basis of this code is provided in Reference 19. A good presentation of the numerical procedures associated with a large family of CFD codes including the PHOENICS code is available in the text by Patanker [20].

The standard k-ε turbulence model, the basis of which is presented above for cylindrical coordinate systems, was employed in computational analyses of simple geometry (Fig. 2) TAD flows. A 20 x 30 grid was employed in these analyses as displayed between planes BB and CC of Figure 3. In all simple TAD configuration analyses, inlet plane velocity, turbulent kinetic energy, and dissipation rate conditions were specified. A constant exit plane (CC in Fig. 3) pressure was prescribed and boundary condition closure was achieved by assuming zero velocity field gradients in the exit plane.

The Pourahmadi and Humphrey [9,10] extension of the standard model was also implemented. As discussed above, this modified turbulence model incorporates the effects of streamline curvature and pressure strain in the fluid by using a variety of approximations to reduce the Reynolds stress transport equations to a set of algebraic equations. Because of the complexity of the algebraic manipulations employed, only a brief outline of the model derivation and implementation is presented below. The reader is referred to the original work in Reference 9 for a detailed development.

The derivation starts from a high Renolds number form of the $\overline{u_i u_j}$ transport equation [9] characterized by the general form shown in equation (11).

$$\frac{D\,\overline{u_i u_j}}{Dt} = P_{ij} + \varepsilon_{ij} + \Pi_{ij} + D_{ij} \qquad (11)$$

The development then proceeds in the following stepwise manner.

1) The $\overline{u_i u_j}$ transport equations are reduced to a system of algebraic equations by invoking a variety of approximations including:

A) Rotta's [12] return to isotropy principle in Π_{ij}

B) Launder, Reece and Rodi's [13] expression for the contribution to Π_{ij} from interaction between mean strain and fluctuating velocities

C) Daly and Harlow's [14] correction to Π_{ij} due to wall effects

D) Gibson and Launder's [15] correction to Π_{ij} due to wall effects

E) Rodi's [11] assumption that $\overline{u_i u_j}/k$ is constant throughout the flow field.

2) The resulting system of algebraic equations is solved for the turbulent stresses.

3) The Boussinesq approximation is then employed, transforming the solution into an algebraic relation for C_μ.

4) The turbulent energy production term is rearranged into the form

$$(k/\varepsilon)U_{\theta,r} = g(P_d/\varepsilon,\ U_\theta/r,\ U_{i,j})/\sqrt{C_\mu}$$

where g is a complex function of the quantities indicated, including the various partials of the mean velocity, $U_{i,j}$.

5) The relation for $(k/\varepsilon)U_{\theta,r}$ from step 4 is substituted into the algebraic relation for C_μ from step 3. Simplification of the resulting expression leads to the cubic polynomial relation

$$F(\sqrt{C_\mu}) = C_\mu^{3/2} + a_1 C_\mu + a_2 C_\mu^{1/2} + a_3 = 0 \qquad (12)$$

where $a_1, a_2, a_3 = a_1, a_2, a_3(P_d/\varepsilon,\ U_\theta/r,\ f,\ U_{i,j})$.

6) The wall correction function f presented in Reference 13 and appearing in step 5 is modified to the form

$$f = \frac{k^{3/2}}{C_w \varepsilon}\left[\frac{1}{y} + \frac{(y/D)^m}{D-y}\right] \qquad (13)$$

thereby permitting asymmetric wall corrections to the pressure strain. In this expression, the asymmetry measure m appears as a new empirical constant.

7) Following Bradshaw [8], the expression for dissipation at near wall nodes is modified by a multiplicative factor of $1/[1\pm\beta U_\theta/(U_{\theta,r}r)]$ in order to introduce the influence of extra strain curvature on the magnitude of the near wall turbulence length scale. This expression also contains a new empirical constant, β.

Suggested values for constants m and β are 7.95 and the order of 10 respectively.

Although the complex development terminating at equation (12) is quite impressive, an unfortunate algebraic error is made in establishing the roots of this equation. Instead of a single positive real root for $\sqrt{C_\mu}$ as predicted in References 9 and 10, multiple real roots, not necessarily positive, can (and did) occur in practice. The implemented version of the Pourahmadi and Humphrey modification included a corrected method of solving for the curvature dependent values of $\sqrt{C_\mu}$. Adding to the difficulties associated with this implementation was the need to prescribe a selection criterion for regions in which multiple roots occurred. This problem was never resolved with complete success as will be discussed more fully in the next section of this report.

In order to more fully understand the elliptic character of developing TAD flows, analyses utilizing an orthogonal body-fitted coordinate (BFC) reference system on an expanded duct geometry were performed. Two such analyses were performed; one on the full geometry, 20 x 80 grid system depicted in Figure 3, and a second on a reduced geometry 20 x 60 grid depicted between planes AA and CC of the same figure. In each case the 20 x 30 grid configuration of the simple TAD analyses was preserved in the region bounded by surfaces BB and CC in Figure 3. In this manner comparison of results using both simple TAD configurations and expanded BFC geometries was facilitated.

Numerical computations employing the grid configuration of Figure 3 were performed utilizing the BFC option of the PHOENICS computer code described in Reference 21. Although potentially more accurate non-orthogonal grid specifications could have been implemented within the framework of the PHOENICS code, direct comparison with results of simple cylindrical system analyses would have then become more difficult. An excellent comprehensive review of methods to numerically generate curvilinear coordinate systems with coordinate lines coincident with boundary segments is given in Reference 22.

RESULTS

Results of this investigation can be separated into three categories dependent upon coordinate reference frame and turbulence model employed. Analyses 1, 2, and 6 described in Table 1 were performed on simple TAD geometries using a cylindrical coordinate system and a standard k-ε turbulence model [17]. In analysis 3 the modified k-ε model of Pourahmadi and Humphrey [9,10], with the correction discussed in the previous section, was employed. The simple TAD geometry displayed in Figure 2 was maintained. Analyses 4 and 5 employed orthogonal BFC reference systems with a standard k-ε turbulence model. The grid system depicted in Figure 3 was used in analysis 4. The same grid pattern, restricted to the corresponding

analysis geometry, was employed in all cases. In addition, the flow Reynolds number was fixed at 10^6 and a curvature ratio $R_c/D = 1$ was prescribed. These values obviously refer to a high rate flow with extremely sharp curvature. A complete summary of the computational analyses of this study is presented in Table 1.

TABLE 1. ANALYSES SUMMARY

Analysis No.	Reference Frame	Figure 2 I/O Planes	Grid	Inlet U Profile	Turbulence Model
1	Cyl.	BB/CC	20 x 30	Plug	k–ε
2	Cyl.	BB/CC	20 x 30	FDP	k–ε
3	Cyl.	BB/CC	20 x 30	Plug	Modified k–ε
4	BFC	AA/EE	20 x 80	Plug	k–ε
5	BFC	AA/CC	20 x 60	Plug	k–ε
6	Cyl.	BB/CC	20 x 30	Plane BB from 5	k–ε

Analyses Constants: $Re = 10^6$ $R_c/D = 1.0$

Turbulence Inlet Conditions
For Plug Inlet U Profile : $k/\bar{U}^2 = 0.005$

$\varepsilon/(\bar{U}^3/D) = (0.005)^{3/2}/0.01$

Exit Plane Pressure: Uniform across exit plane

In Figures 4, 5, and 6 are displayed developing profiles of velocity, pressure, and turbulent kinetic energy respectively, for the case of a simple TAD geometry with inlet plug flow. In response to the strong cross stream pressure gradients evident throughout the flow domain, the velocity profiles are observed to become increasingly asymmetric. The most substantial pressure adjustments occur within the final 30 deg of duct travel, and in response there is a significant acceleration of flow near the outer wall with a corresponding deceleration near the inner, convex, duct wall. The net effect is a nearly linear velocity profile very near the exit plane reminiscent of a solid body rotation. Quantitatively, the near exit plane velocity varies from just under 25 percent to somewhat over 140 percent of the average flow velocity. In the entrance region of the duct, the plug flow characteristic is observed to persist virtually unchanged past the midplane (θ = 90 deg) of the duct. The large cross stream pressure gradient predicted for the TAD inlet region together with the specified plug flow entrance velocity profile is suggestive of a very large swirl chamber feed to the TAD. This type of configuration is of course not prevalent in rocket engine or turbomachinery applications.

The turbulent kinetic energy profiles displayed in Figure 6 exhibit rapid decay in the plug flow core region as expected. An initial decay in the near wall turbulent

kinetic energy is followed by a significant rise in the accelerating concave wall region, and a continuing gradual decay in the decelerating convex wall region. Near the exit plane, the turbulent energy profile develops the knee observed [1,2] and predicted [10] in previous curved duct investigations conducted at smaller values of Re and R_c/D.

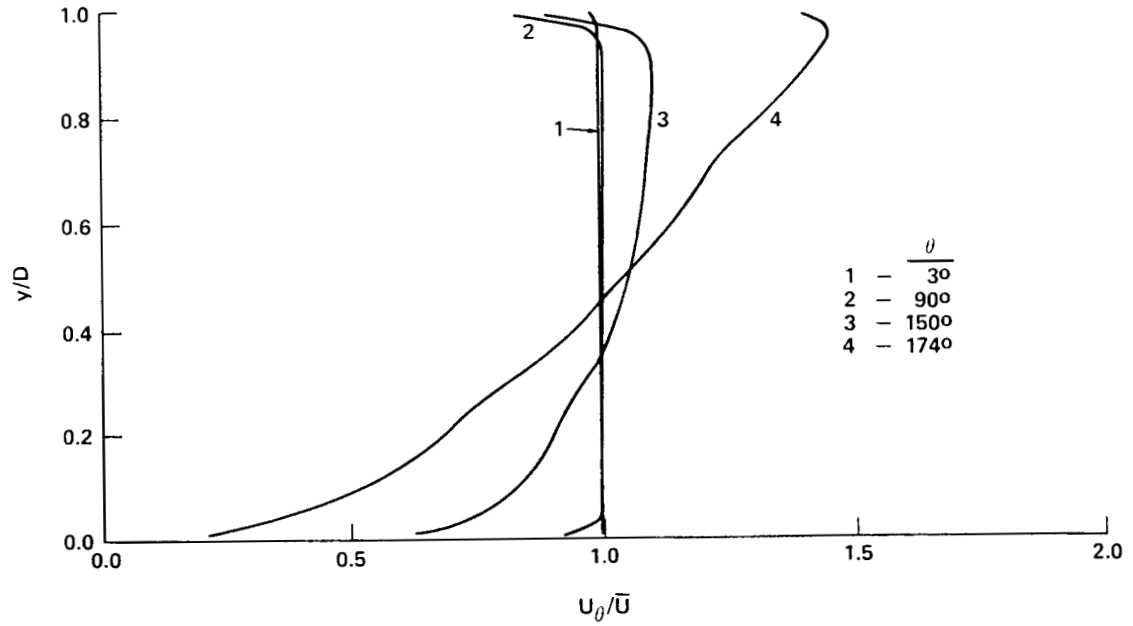

Figure 4. Streamwise velocity profiles for simple TAD geometry with plug flow inlet: Analysis 1.

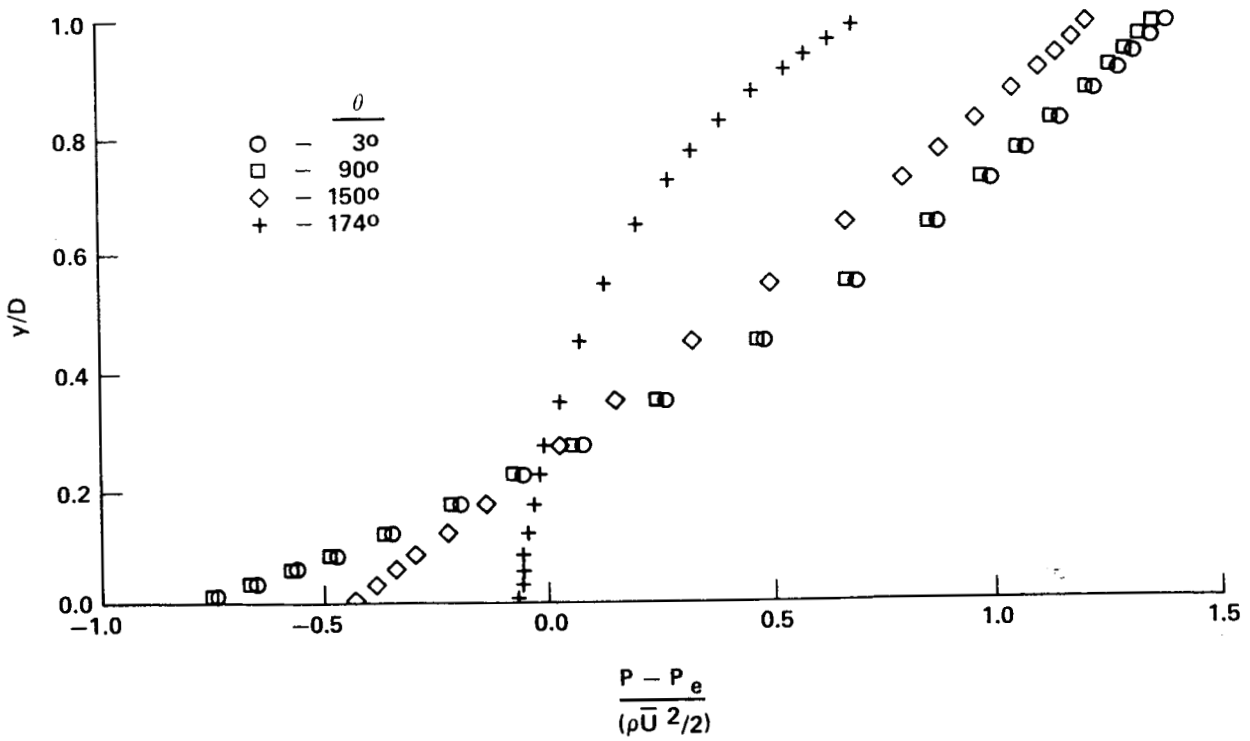

Figure 5. Pressure profiles for simple TAD geometry with plug flow inlet: Analysis 1.

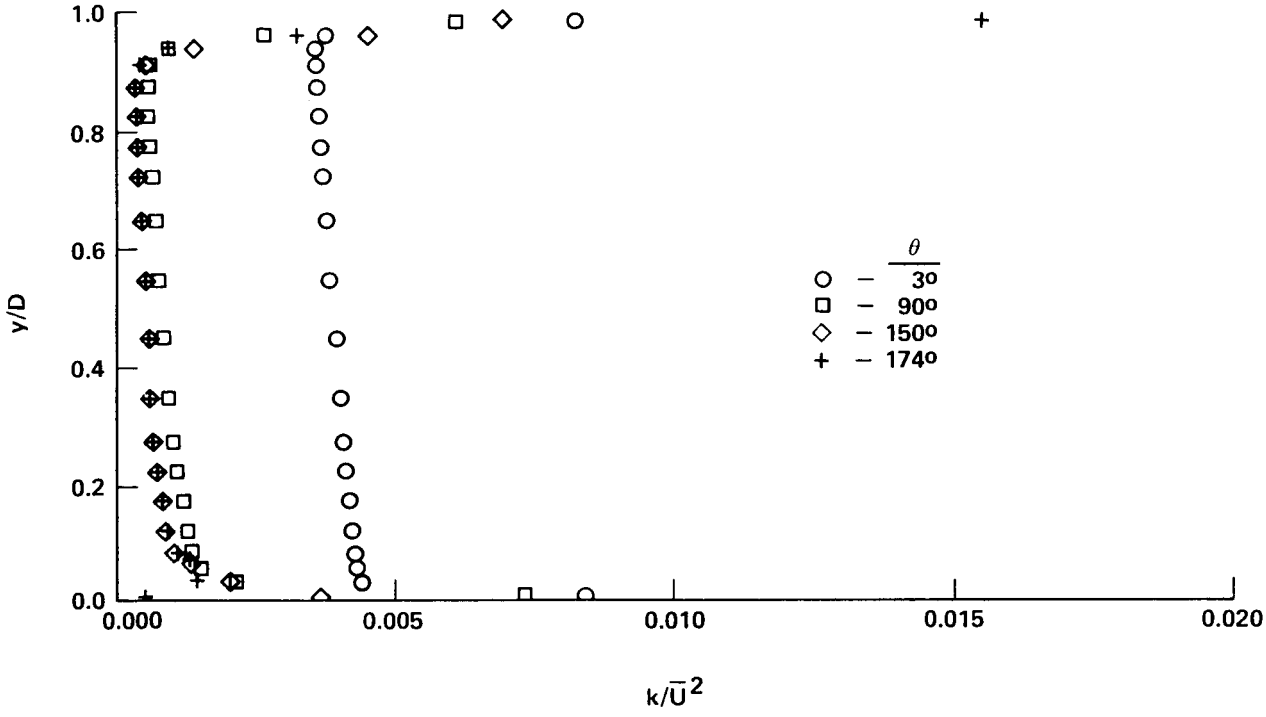

Figure 6. Turbulent kinetic energy profiles for simple TAD geometry with plug flow inlet: Analysis 1.

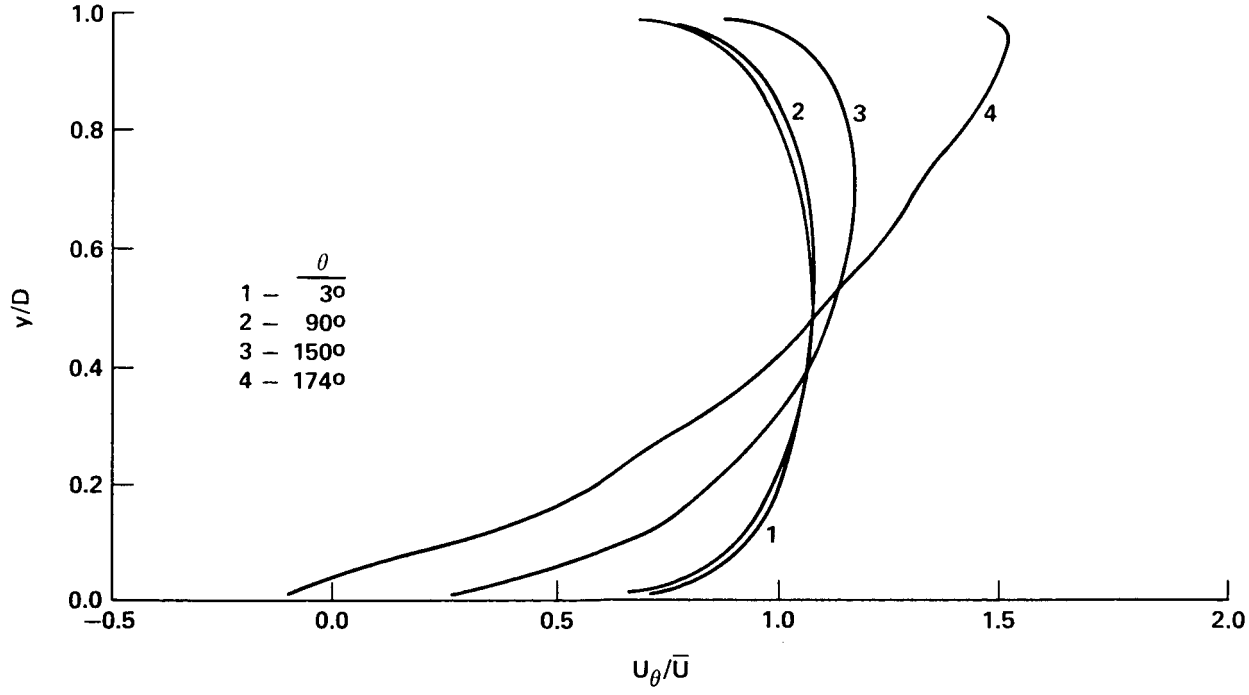

Figure 7. Streamwise velocity profiles for simple TAD geometry with FDP flow inlet: Analysis 2.

Results of a simple TAD geometry analysis with a fully developed turbulent duct flow inlet condition are displayed in Figures 7, 8, and 9. The general shape characteristics and scale of the pressure profiles in Figure 8 are similar to the previous plug flow inlet case. The development sequence for the velocity profiles is also similar to the analysis 1 case with little profile adjustment prior to the 90 deg midplane of the TAD, and significant velocity gradient increases and profile linearization in the rapid adjustment exit region. The salient feature displayed in Figure 7 is the appearance of a recirculation region near the inner wall of the duct. This region extends back somewhat over 6 deg from the exit plane and occupies approximately 4 percent of the duct cross section at the exit plane. The occurrence of a negative velocity region in the exit plane presents certain difficulties involving computational error as discussed in Reference 21. Despite this problem, flow separation from the inner convex wall is predicted to occur between θ = 171 deg and θ = 174 deg. This phenomena is not observed to occur in less sharply curved channels with smaller values of the flow Reynolds number [1,2,6].

The turbulent kinetic energy profiles depicted in Figure 9 differ substantially from the plug flow inlet case both in shape and development history. The initial profile shape is symmetric and of the same magnitude as displayed for the analysis 1 entrance profile. Because of the entrance cross stream velocity gradients present in the FDP entrance case, however, the turbulent kinetic energy is predicted to increase significantly in the flow direction away from the convex wall. This is in sharp contrast to the rapid post entrance decay of k exhibited in Figure 6 for the plug flow inlet case. Near the exit plane, cross stream velocity gradients and the energy dissipation rate away from the convex wall increase rapidly in the flow direction, and the increase in turbulent energy is arrested. In the vicinity of the convex wall there is a substantial adverse pressure gradient leading to deceleration and, as the exit plane is approached, flow separation. This is accompanied by a sharp decrease in the inner wall region values of k.

Direct comparison of the downstream velocity and pressure profiles predicted in analyses 1 and 2 are displayed in Figures 10 and 11. The similarities in each of the profile pairs is obvious. The near exit plane pressure adjustment is predicted to occur more suddenly in the case of plug flow inlet conditions. It is evident that the inner wall characteristics of the near exit plane flow are substantially affected by changes in the inflow boundary conditions.

In the third analysis of the computational sequence, the modified k-ε model of Pourahmadi and Humphrey [9,10] was implemented in the user definition section of the PHOENICS routine. Severe difficulties were initially encountered in attempts to obtain reasonable solutions. Further investigation revealed the equation (12) rooting error described previously.

In the context of the PHOENICS implementation, the Pourahmadi and Humphrey [9,10] modification for a specific finite difference cell P requires manipulation of the staggered grid velocity vectors indicated in Figure 12. In addition, grid distances from each of the indicated neighboring cells to the P cell boundaries are needed together with estimates of k and ε at P. The entire manipulation was computationally intense, often tripling the clock time of analysis.

Despite the increased computational effort, convergence difficulties were repeatedly encountered. The source of the problem was the behavior of the polynomial $F(\sqrt{C_\mu})$, the roots of which indicate candidate values of C_μ. Typical $F(\sqrt{C_\mu})$ loci are depicted in Figure 13. These polynomial traces were arrived at by

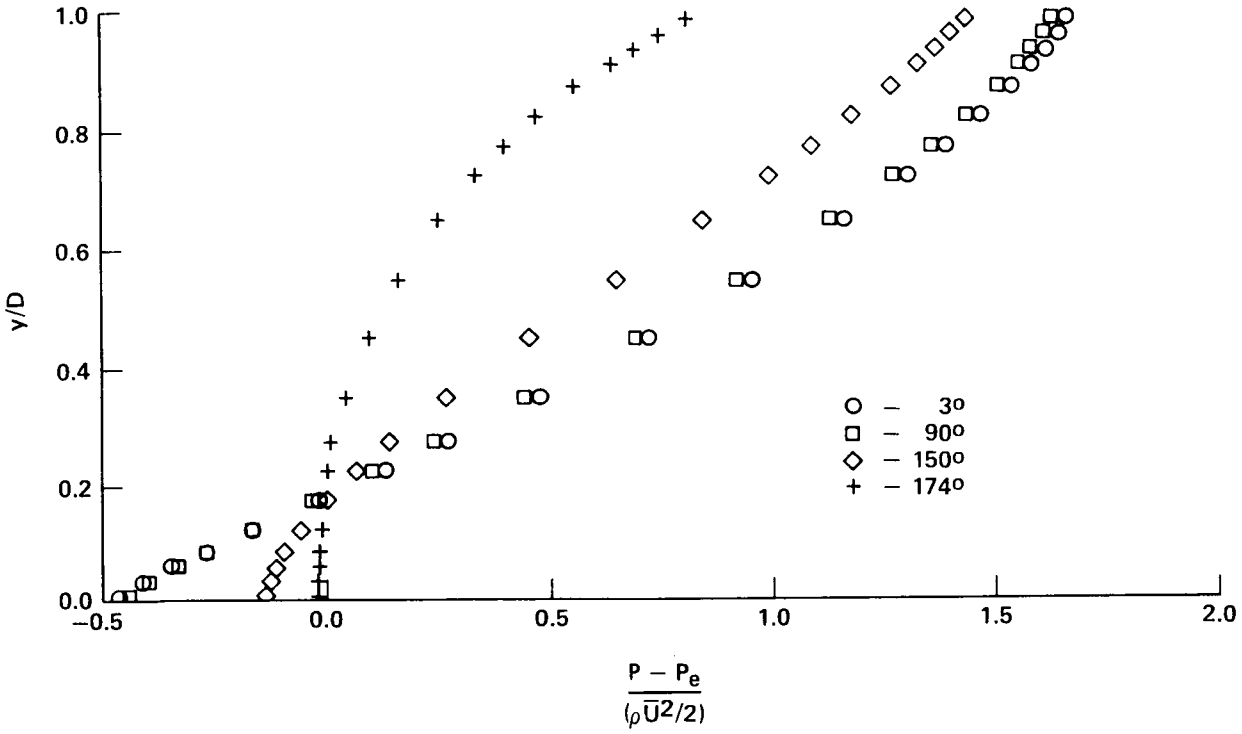

Figure 8. Pressure profiles for simple TAD geometry with FDP flow inlet: Analysis 2.

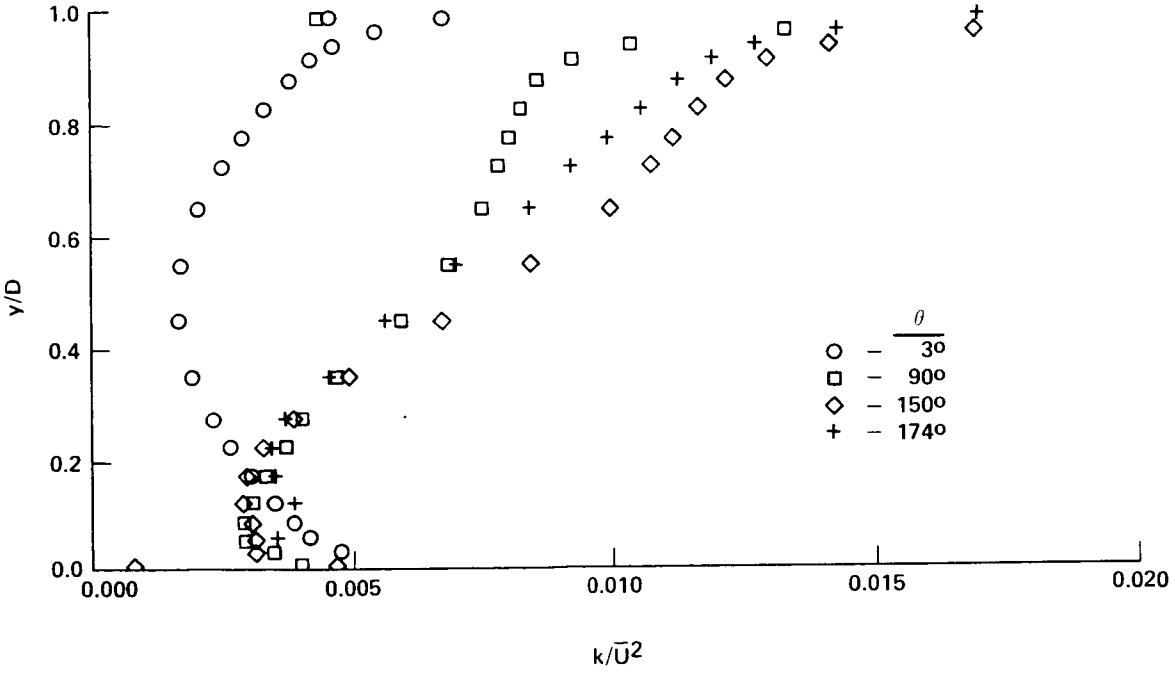

Figure 9. Turbulent kinetic energy profiles for simple TAD geometry with FDP flow inlet: Analysis 2.

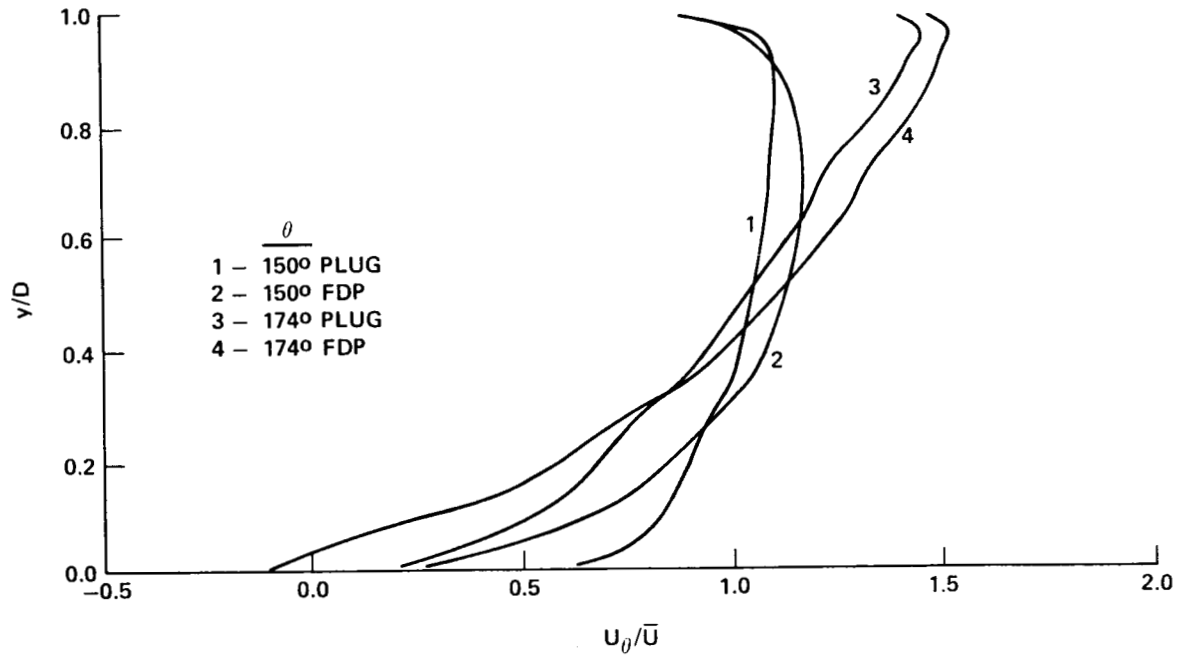

Figure 10. Streamwise velocity profile comparisons for simple TAD geometry.

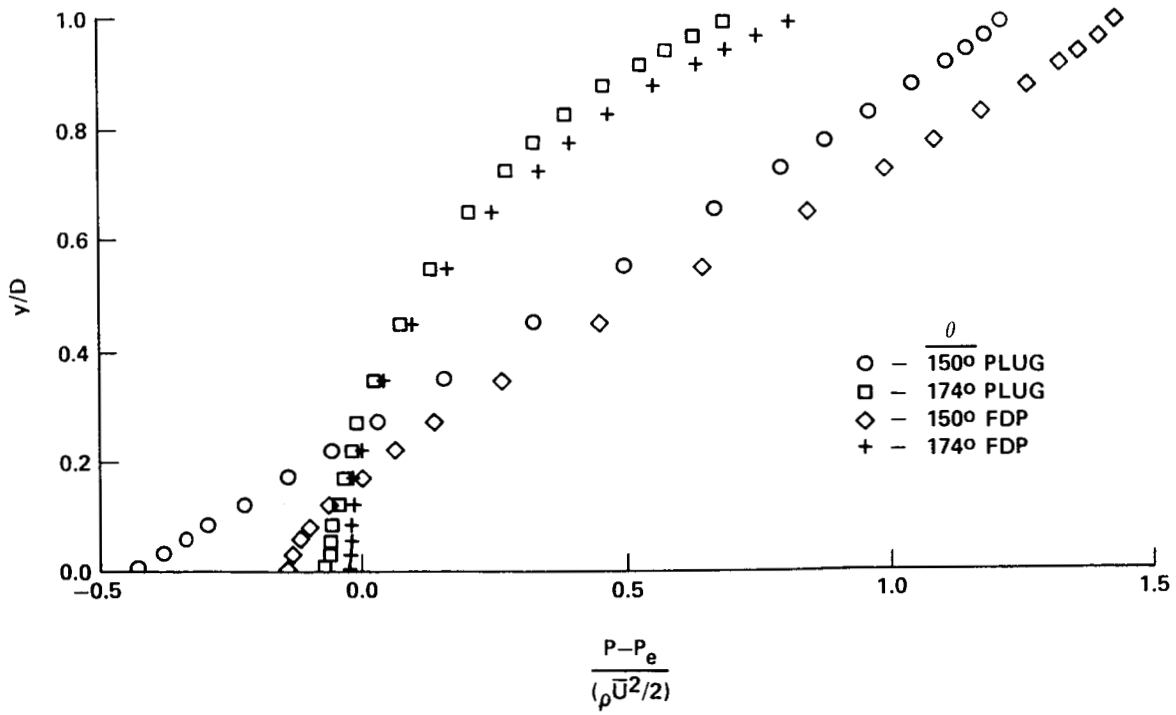

Figure 11. Pressure profile comparisons for simple TAD geometry.

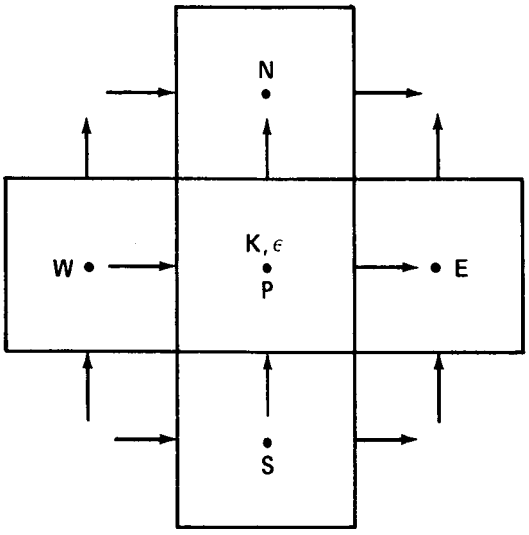

Figure 12. Pourahmadi and Humphrey model [9,10] staggered grid basis cell.

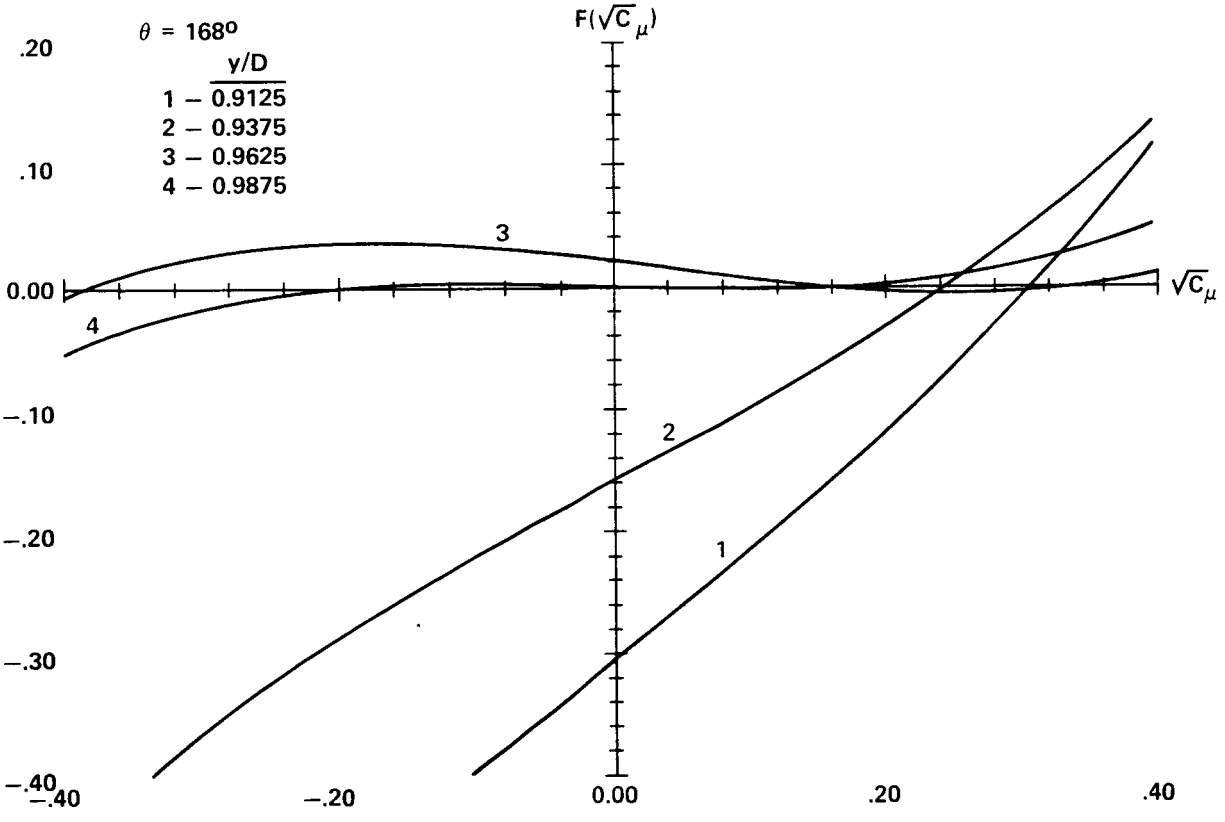

Figure 13. Behavior of $F(\sqrt{C_\mu})$ polynomial at various cross stream locations for θ = 168 deg: Analysis 3.

computationally testing the modified k-ε turbulence model on a simple TAD geometry, plug inlet flow problem. Analysis 3 as described in Table 1 was initiated at the standard k-ε model solution value of analysis 1. An intermediate flow field result was determined by arbitrarily selecting the principal theta transformation root of the cubic polynomial $F(\sqrt{C_\mu})$ whenever multiple roots occurred. The trigonometric or theta transformation method for determining roots of a cubic polynomial is described in most mathematical handbooks (see for example Reference 23).

It is evident from Figure 13 that for θ = 168 deg, the near concave wall behavior of F was that of a cubic polynomial with multiple real roots. This behavior was not isolated, occurring irregularly throughout the flow field and frequently in near wall regions. Unfortunately it is in these near wall regions that the modified k-ε model was expected to yield its most meaningful results [9,10]. The behavior of the $F(\sqrt{C_\mu})$ polynomial at y/D = 0.9875 (the node closest to the concave wall) was particularly disturbing. As indicated in Figure 13, the trace of F was virtually colinear with the C_μ axis for $-0.2 < C_\mu < 0.2$. Three distinct real roots were determined at this nodal position, however, the ill natured character of F is apparent, making the computational process extremely susceptible to even small numerical errors.

Near exit plane values of C_μ were determined as shown in Figure 14. It should be noted that the line of C_μ = 0.09, the standard k-ε model value, occurring at θ = 150 deg was an assigned default value selected whenever the cross stream velocity gradient became small. Small values of $U_{\theta,r}$ led to extreme variation of the $F(\sqrt{C_\mu})$ polynomial, hence the default selection in these regions. Pourahmadi and Humphrey [9,10] also note the ill behavior of C_μ in the core region of the duct. They attribute this behavior to a breakdown in the assumption that $\overline{u_i u_j}/k$ is constant in this region. Their reasoning is less than compelling. It is entirely possible that the problem of determining reasonable values for C_μ is completely numerical, and that consideration of a more primitive implicit form of the C_μ relation might yield stable results across the entire duct cross section.

Recognizing that the analysis 3 results are only intermediate, lacking a completely acceptable method of selecting C_μ, it is useful and interesting to observe position dependent characteristics of the variant C_μ. In Figure 14, for θ = 174 deg, C_μ is observed to take on values substantially less than the standard value of 0.09 in near wall regions, rising to nearly 0.09 just outside the convex wall region and then falling to near zero in the flow core, rising again to near the standard value and well beyond just outside the concave wall region. Figure 15 displays the near concave wall behavior of C_μ throughout the flow domain. It is evident that the near wall node value of C_μ remains essentially constant at around 0.03 throughout while the adjacent node value of C_μ took on default values near the TAD entrance, rising dramatically to a value of nearly 0.4, and then falling steadily to a value in excess of 0.1 before rising dramatically near the duct exit. The turbulent kinetic energy profiles displayed in Figure 16 exhibit the same qualitative character as the unmodified k-ε model profiles of Figure 6 except that near outer wall k values are greatly magnified and exhibit a knee as the wall is approached. Details of the near convex wall comparisons of turbulent kinetic energy are shown in Figure 17. Both the

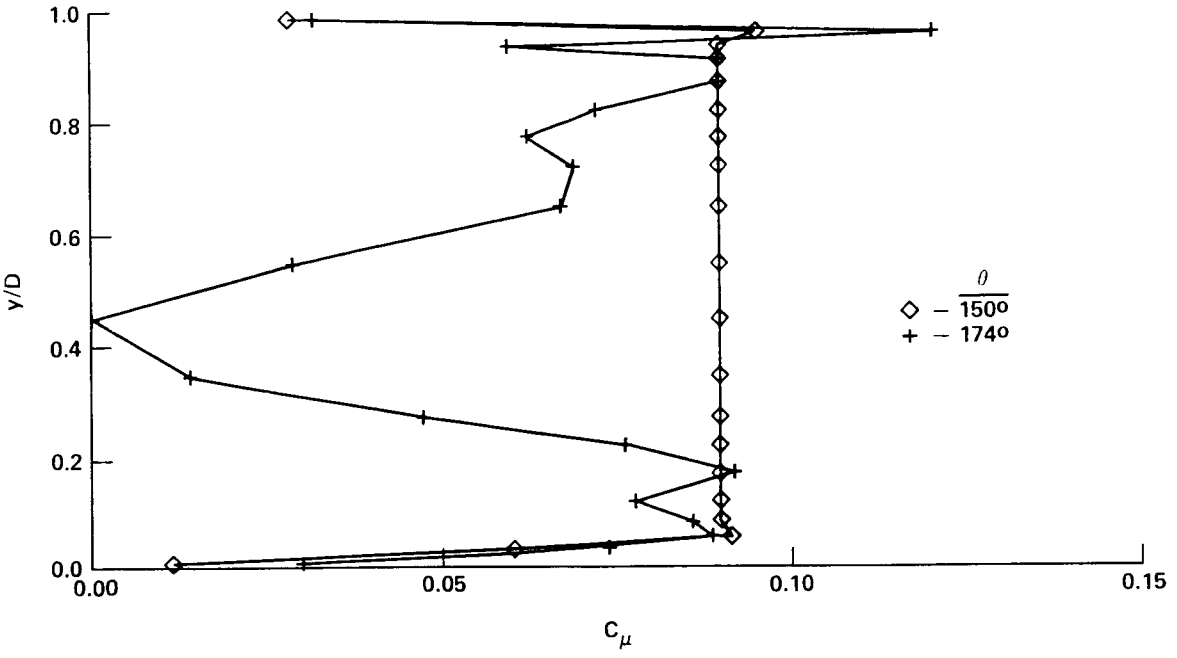

Figure 14. Characteristic C_μ profiles for simple TAD geometry with plug flow inlet condition using the modified k-ε model: Analysis 3.

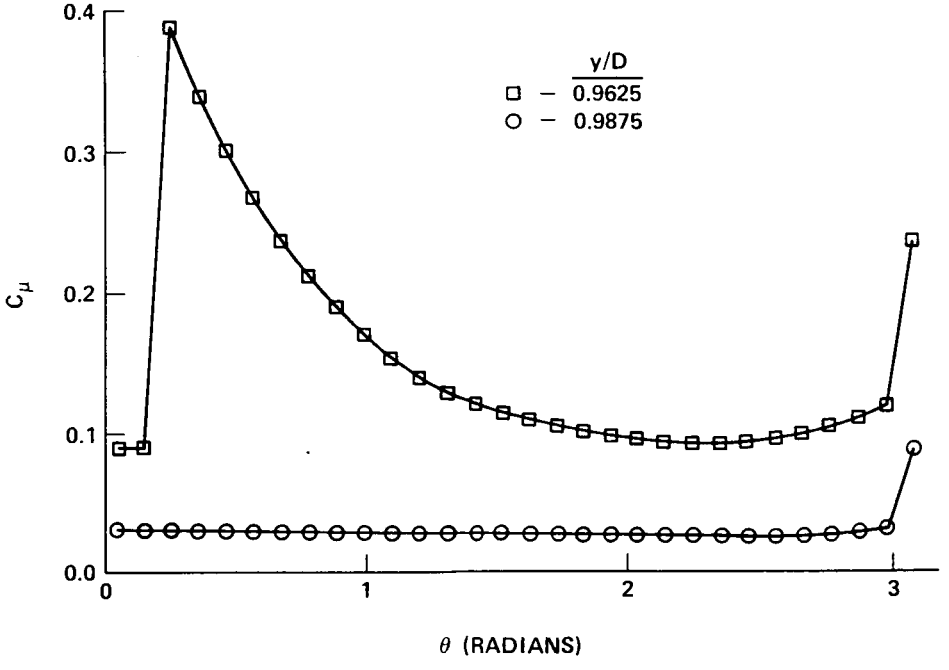

Figure 15. Streamwise variation of C_μ close to the concave wall: Analysis 3.

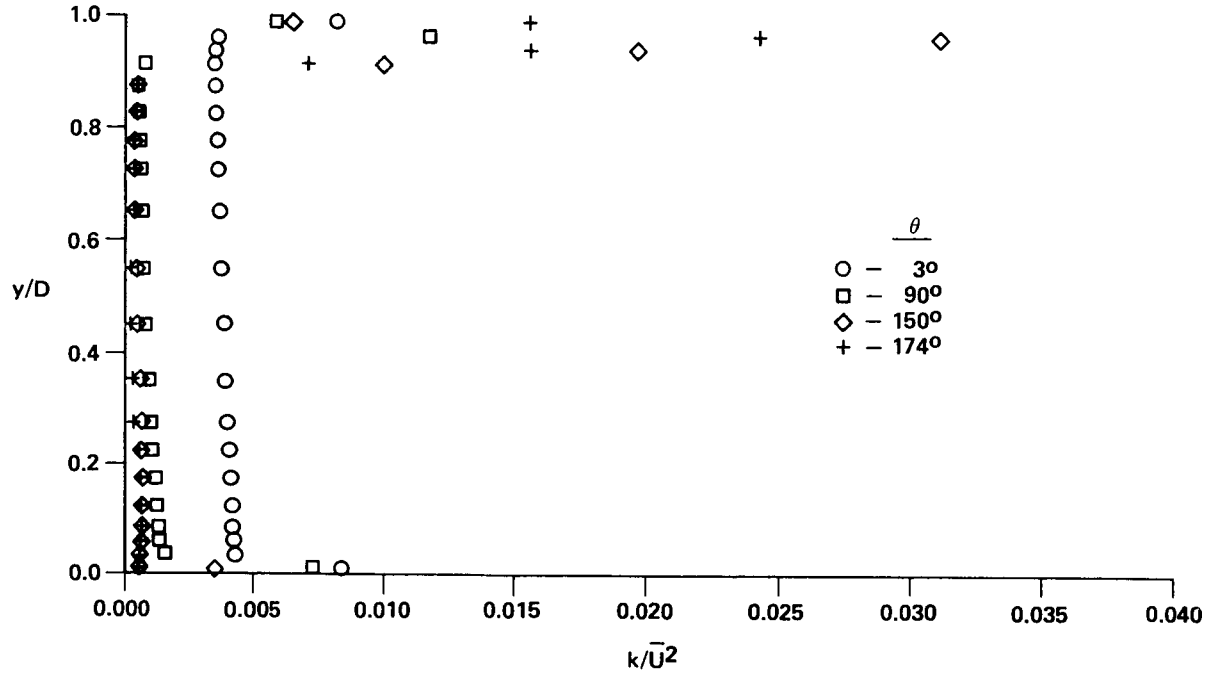

Figure 16. Turbulent kinetic energy profiles for simple TAD geometry using the modified k-ε model: Analysis 3.

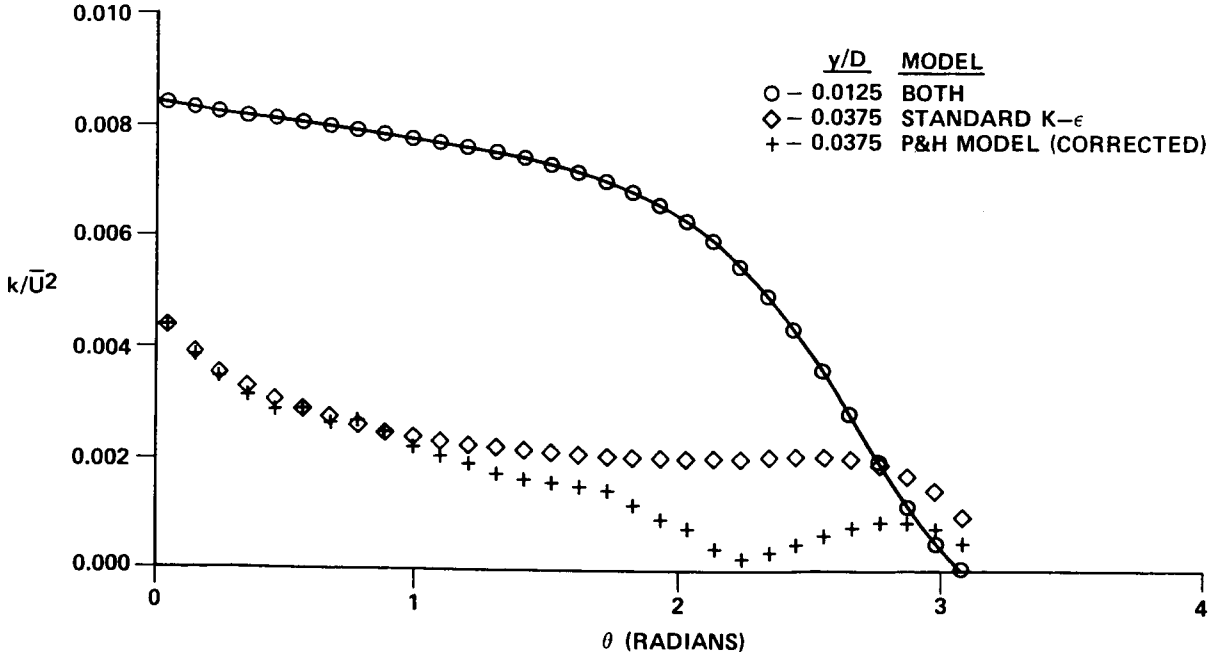

Figure 17. Comparison of near wall turbulent kinetic energy predictions.

standard and modified k-ε models predict the same k values at the adjacent wall node, however, modified model kinetic energy predictions were somewhat smaller than standard at the neighboring y node near the duct exit. Estimated velocity and pressure profiles obtained using the modified k-ε model were virtually identical to standard model results.

Two separate BFC computational analyses were performed in order to explore the elliptic character of the TAD flow field. These are described in Table 1, analyses 4 and 5. Before describing results of these studies, several general observations are warranted. First, the early version of the SSME TAD geometry depicted in Figure 1 suggests a computational model with a short entrance region and a relatively long straight exit region. In Figure 3 this would indicate flow entrance at plane EE and exit at plane AA. Several attempts at such an analysis using the BFC option of the PHOENICS computer code were unsuccessful. This does not necessarily indicate a shortcoming in the PHOENICS/BFC solution technique. It is likely that more extensive experience with judicious selection of the relaxation factors and other heuristic tuning parameters inherent in the PHOENICS code, and indeed any CFD code with like capabilities, would have led to solution convergence with the flow orientation described above. Because of the limited time available to gain computational experience, and because it was found that extension of the straight duct inlet zone greatly enhanced convergence characteristics, the suggested SSME TAD flow orientation was reversed, with the inlet prescribed in plane AA and exit at plane EE.

A second observation concerning the BFC computations involves the degree of solution convergence at analysis termination. Using the absolute residuals sum criterion described more fully in the PHOENICS documentation, the convergence rate at termination had slowed to approximately 0.1 percent of total absolute residuals sum per solution sweep. This rate was achieved after approximately 30 clock hours of computation on the Perkin-Elmer 3220 computer system utilized during this study. Although clock run time is a poor absolute measure of computational efficiency, relative to simple TAD configurations, the BFC analyses required an order of magnitude more clock run time and at best achieved an absolute residuals sum convergence measure a full order of magnitude larger than the simple TAD analyses. Noting that the BFC grid patterns were approximately three times the size of the simple cylindrical system TAD grids, it is obvious that the BFC analyses were relatively high overhead computations. In addition, because calculation was interrupted before achieving a proportionately small convergence measure, results of the BFC analyses are considered to yield only qualitative predictions of flow field characteristics.

Figures 18, 19, and 20 display results of the analysis 4 BFC computations for TAD inlet/outlet velocity, pressure, and turbulent kinetic energy profiles respectively. These calculations were performed using the full grid pattern displayed in Figure 3 with flow inlet at plane AA. It is evident in Figures 18 and 19 that BFC calculated TAD inlet flow field features are radically different from the inlet boundary assumptions of the simple duct analyses. The inlet velocity profile resembles the 1/r proportionality of ideal fluid flow except in the near wall regions while the outlet profile appears very much like a fully developed turbulent duct flow. Obviously the antisymmetric character of the predicted TAD outlet pressure profile is quite different from the assumed uniform exit plane distribution of the simple geometry analyses. Because of the centrifugally induced cross-stream pressure gradient at the TAD exit, the duct like flow profile at plane CC developed into the stretched, r proportional profile reminiscent of rigid body rotation in the 2 x D straight exit duct. Predicted developing velocity profiles in the exit duct are displayed in Figure 21. In the exit section, the pressure adjusts to the assumed uniform condition at exit plane EE. The core of the TAD exit plane k profile shown in Figure 20 resembles the core suppressed

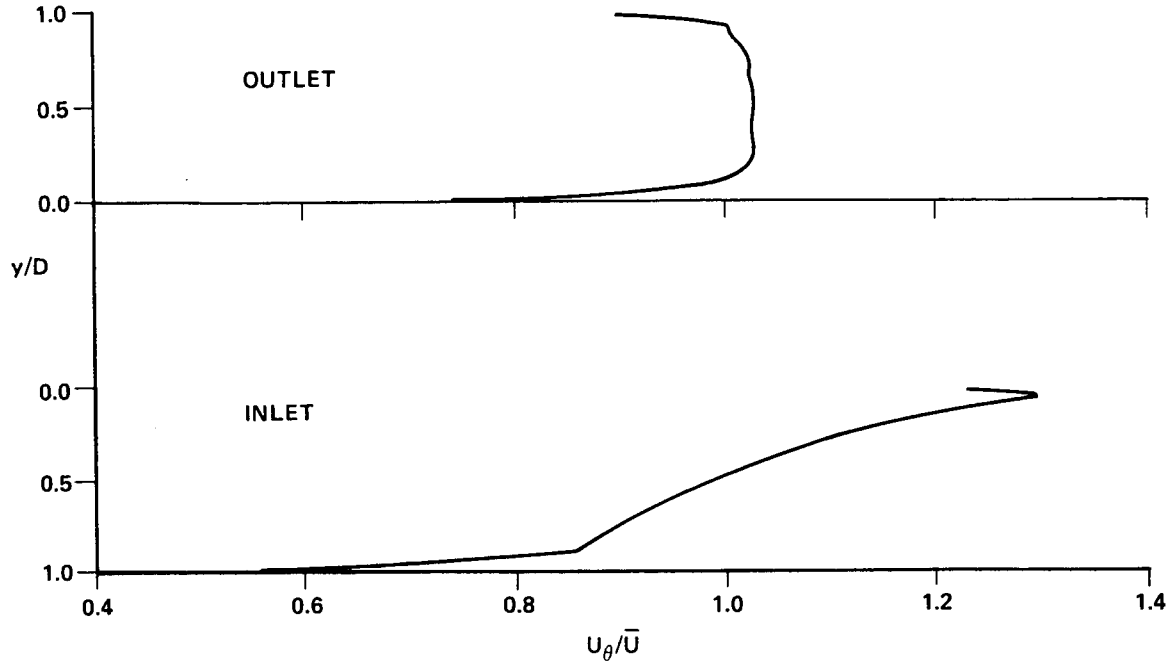

Figure 18. TAD I/O velocity profiles for BFC computation: Analysis 4.

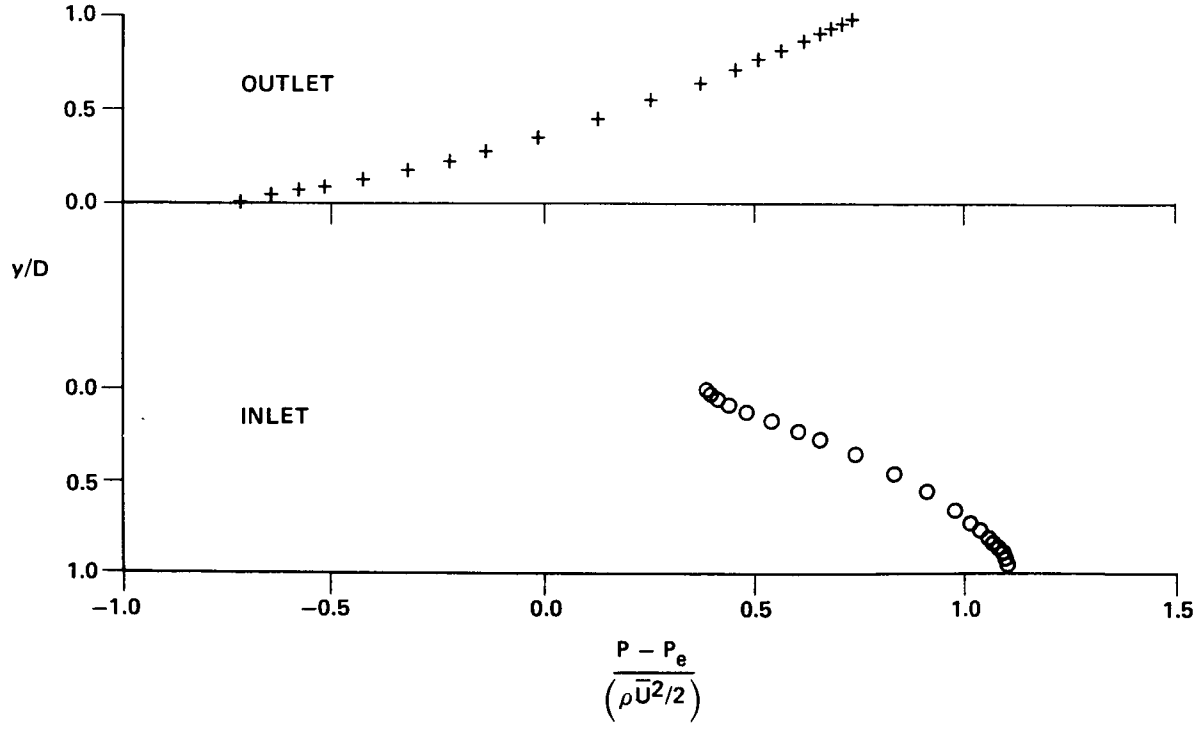

Figure 19. TAD I/O pressure profiles for BFC computation: Analysis 4.

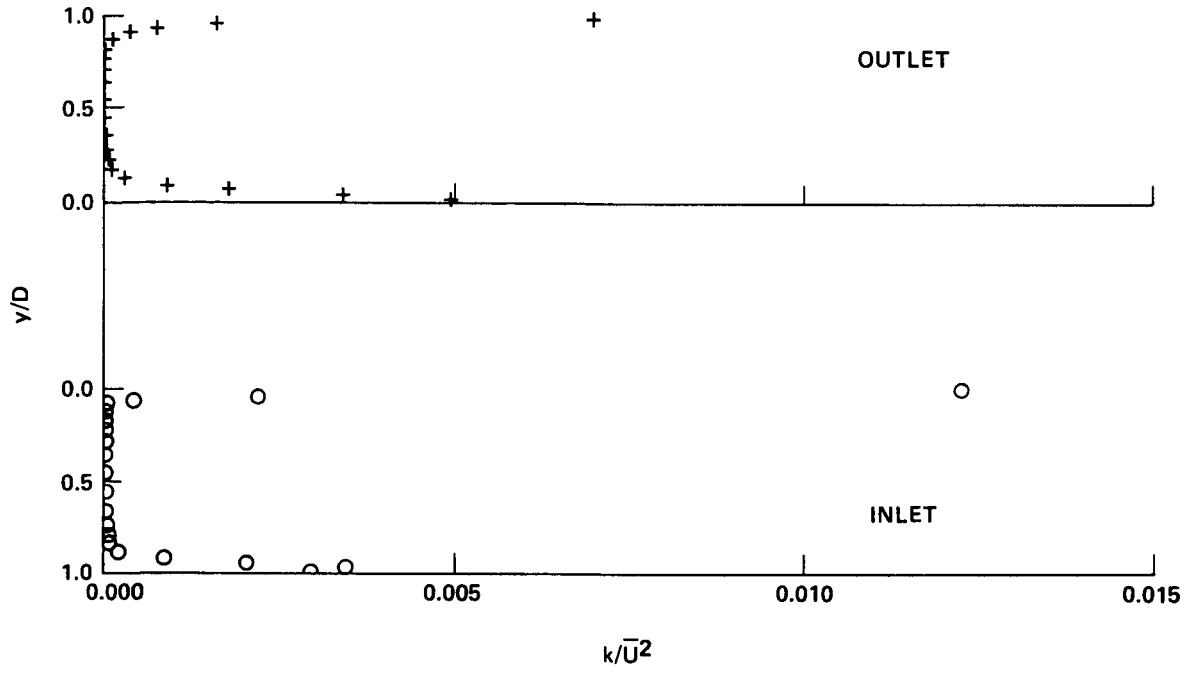

Figure 20. TAD I/O turbulent kinetic energy profiles for BFC computation: Analysis 4.

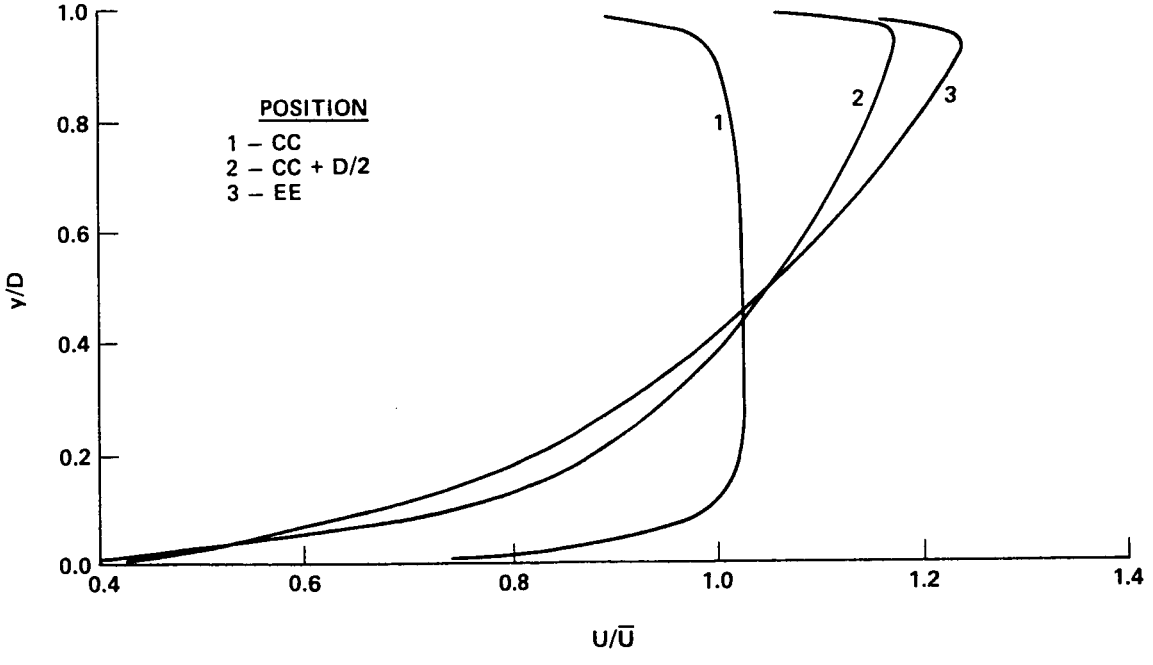

Figure 21. Developing velocity profiles in the straight 2 x D exit section of Analysis 4.

profile of the simple geometry analysis with plug flow inlet conditions displayed in Figure 6. No inner wall knee is observed in the BFC k predictions, however, outer wall turbulent kinetic energies are reduced in the BFC analysis.

In order to reinforce the extended geometry predictions of analysis 4, a comparison test was devised. BFC analysis 5 was run on the reduced configuration between planes AA and CC. Plug flow inlet conditions were prescribed at plane AA and uniform exit plane pressure was assumed. Results of this computational procedure at the TAD entrance plane BB were used as boundary conditions for a simple geometry analysis using a cylindrical system with the same uniform exit plane pressure assumed. Predictions of analysis 5 and 6 should have been identical, at least theoretically. Unfortunately, there was a substantial discrepancy in the predicted flow field characteristics as demonstrated in Figures 22 and 23. Even considering the qualitative nature of the BFC analysis, the comparisons were disturbing. Cylindrical system predictions of cross-stream velocity gradients at the exit plane were generally much larger than results using BFC analysis as is evident in Figure 22. In addition, a rather large recirculation zone was predicted using the traditional cylindrical coordinate system analysis. Inner wall flow separation was predicted approximately 24 deg from the exit plane, with the counterflow velocity zone extending into the fluid over 7.5 percent of the duct width at the exit plane. By contrast, the near inner wall node velocity at the exit plane, obtained using BFC computations was over 40 percent of the average velocity. Pressure profiles from the two analyses at the TAD entrance plane were not even similar in character, as displayed in Figure 23.

If the standard cylindrical system analysis is presumed correct, based on an extensive history of computational success and better convergence characteristics, then the reliability of the current PHOENICS BFC option must be suspect. This conclusion must, however, be tempered by the fact that acceptable convergence was attained with cylindrical system analysis while only run time constrained convergence was achieved using BFC's. In addition, in order to prevent divergence of the PHOENICS based computational procedure involving BFC's, it was necessary to neglect certain curvature contributions in the finite difference approximations. The rationale for neglect of these terms is more fully described in the PHOENICS BFC documentation [21], however, for curvature dominated flows, such as that occurring in the SSME TAD, neglect of such contributions is dissatisfying. Only by further computational study and experimental comparison can deficiencies in the approximation procedure be adequately quantified.

CONCLUSIONS

1) The curvature modified k-ε turbulence model developed by Pourahmadi and Humphrey [9,10] cannot be utilized as presented due to algebraic errors in the $F(\sqrt{C_\mu})$ rooting scheme.

2) A corrected version of the Pourahmadi and Humphrey [9,10] curvature modified turbulence model has potential if an adequate method of selecting the multivalued root $\sqrt{C_\mu}$ can be determined.

3) Neglect of curvature related terms within the BFC option of the general purpose CFD code PHOENICS yields results inconsistent with the predictions of standard orthogonal systems analyses for sharply curved internal flows.

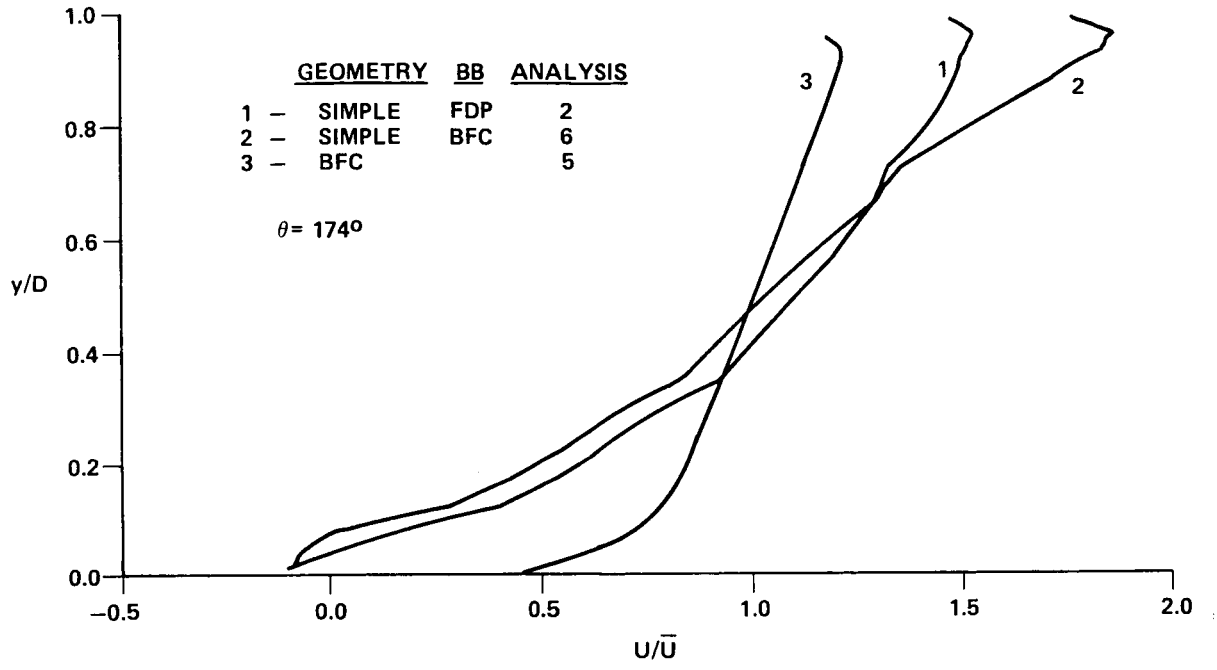

Figure 22. Comparison of TAD outlet velocity profiles.

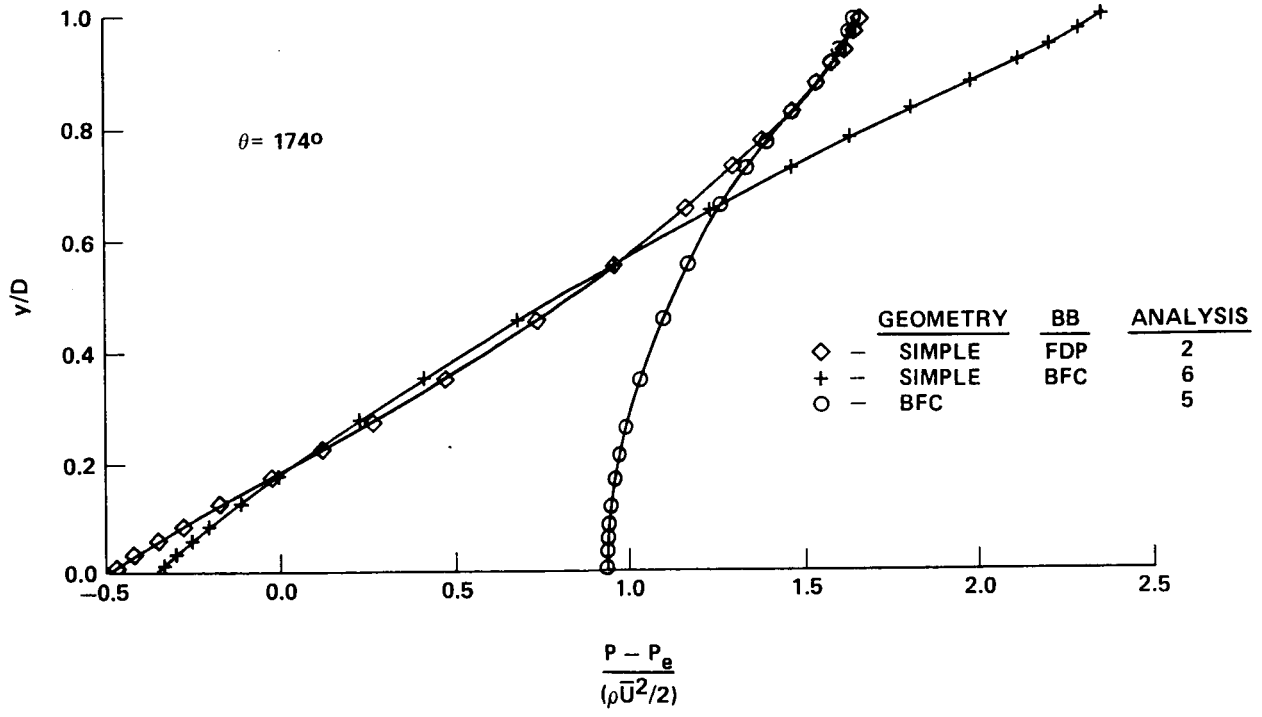

Figure 23. Comparison of TAD inlet pressure profiles.

4) Construction of an acceptable turbulence model for use in the analysis of sharply curved internal flows must await the availability of adequate experimental data, and will require a systematic program of computational verification.

REFERENCES

1. Eskinazi, S. and Yeh, H.: An Investigation of Fully Developed Turbulent Flows in a Curved Channel. Journal of Aeronautical Sciences, 1956, pp. 23-24.

2. Ellis, L. B. and Joubert, P. N.: Turbulent Shear Flow in a Curved Duct. Journal of Fluid Mechanics, Vol. 62, 1974, pp. 65-84.

3. Meroney, R. N. and Bradshaw, P.: Turbulent Boundary-Layer Growth Over a Longitudinally Curved Surface. AIAA Journal, Vol. 13, 1975, pp. 1446-1453.

4. Launder, B. E., Priddin, C. H., and Sharma, B. I.: The Calculation of Turbulent Boundary Layers on Spinning and Curved Surfaces. Trans. ASME, Journal of Fluids Engineering, 1977, pp. 231-239.

5. Brinich, P. F. and Graham, R. W.: Flow and Heat Transfer in a Curved Channel. NASA TN D-8464, 1977.

6. Hunt, I. A. and Joubert, P. N.: Effects of Small Streamline Curvature on Turbulent Duct Flow. Journal of Fluid Mechanics, Vol. 91, 1979, pp. 633-659.

7. Humphrey, J. A. C., Whitelaw, J. H., and Yee, G.: Turbulent Flow in a Square Duct with Strong Curvature. Journal of Fluid Mechanics, Vol. 103, 1981, pp. 443-463.

8. Bradshaw, P.: Effects of Streamline Curvature on Turbulent Flow. AGARDograph No. 169, 1973.

9. Humphrey, J. A. C. and Pourahmadi, F.: A Generalized Algebraic Relation for Predicting Developing Curved Channel Flow with a k-ε Model of Turbulence. University of California, LBL Rept. 12009 Rev., 1981.

10. Pourahmadi, F. and Humphrey, J. A. C.: Prediction of Curved Channel Flow with an Extended k-ε Model of Turbulence. AIAA Journal, Vol. 21, 1983, pp. 1365-1373.

11. Rodi, W.: A New Algebraic Relation for Calculating the Reynolds Stresses. ZAMM, Vol. 56, 1976, pp. T219-T221.

12. Rotta, J. C.: Turbulente Stromumgen. B. G. Teubner, Suttgart, 1972.

13. Launder, B. E., Reece, G. J., and Rodi, W.: Progress in the Development of a Reynolds-Stress Turbulence Closure. Journal of Fluid Mechanics, Vol. 68, 1975, pp. 537-566.

14. Daly, B. J. and Harlow, F. H.: Transport Equations of Turbulence. The Physics of Fluids, Vol. 13, 1970, pp. 2634-2649.

15. Gibson, N. M. and Launder, B. E.: Ground Effects on Pressure Fluctuations in the Atmospheric Boundary. Journal of Fluid Mechanics, Vol. 86, 1978, pp. 491-507.

16. Nakayama, A. and Koyama, H.: A Wall Law for Turbulent Boundary Layers in Adverse Pressure Gradients. AIAA Journal, Vol. 22, 1984, pp. 1386-1389.

17. Launder, B. E. and Spalding, D. B.: The Numerical Computation of Turbulent Flows. Computer Methods in Applied Mechanics and Engineering, Vol. 3, 1974, pp. 269-289.

18. Launder, B. E., Morse, A., Rodi, W., and Spalding, D. B.: The Prediction of Free Shear Flows – A Comparison of the Performance of Six Turbulence Models. Proceedings of NASA Conference on Free Shear Flows, Langley, 1972.

19. Spalding, D. B.: A General Purpose Computer Program for Multi-Dimensional One and Two-Phase Flow. Mathematics and Computers in Simulation, Vol. 23, 1981, pp. 267-276.

20. Patankar, S. V.: Numerical Heat Transfer and Fluid Flow. Hemisphere Publishing Corp., McGraw-Hill Book Co., New York, 1980.

21. Gunton, M. C., Malin, M. R., Rosten, H. I., Spalding, D. B., and Tatchell, D. G.; Use of Body-Fitted-Coordinate Scheme in Phoenics. CHAM TR/97, 1984.

22. Thompson, J. F. and Warsi, Z. U. A.: Boundary-Fitted Coordinate Systems for Numerical Solution of Partial Differential Equations - A Review. Journal of Computational Physics, Vol. 47, 1982, pp. 1-108.

23. Korn, G. A. and Korn, T. M.: Mathematical Handbook for Scientists and Engineers. Second Edition, McGraw-Hill Book Co., New York, 1968.

1. REPORT NO.	2. GOVERNMENT ACCESSION NO.	3. RECIPIENT'S CATALOG NO.
NASA CR-3990		

4. TITLE AND SUBTITLE	5. REPORT DATE
Turbulent Flow Field Predictions in Sharply Curved Turn-Around Ducts	June 1986
	6. PERFORMING ORGANIZATION CODE
7. AUTHOR(S)	8. PERFORMING ORGANIZATION REPORT #
L. Michael Santi	
9. PERFORMING ORGANIZATION NAME AND ADDRESS	10. WORK UNIT NO.
Memphis State University Memphis, Tennessee	M-529
	11. CONTRACT OR GRANT NO.
	NGT-01-008-021
12. SPONSORING AGENCY NAME AND ADDRESS	13. TYPE OF REPORT & PERIOD COVERED
National Aeronautics and Space Administration Washington, D.C. 20546	Contractor Report
	14. SPONSORING AGENCY CODE

15. SUPPLEMENTARY NOTES

Prepared for Atmospheric Science Division, Systems Dynamics Laboratory, George C. Marshall Space Flight Center, Marshall Space Flight Center, Alabama.

16. ABSTRACT

In this investigation, two-dimensional turbulent flow of incompressible Newtonian fluids in sharply curved 180 deg turn around ducts is studied. Results of an approximate numerical flow field analysis utilizing an orthogonal, body-fitted, curvilinear coordinate system are compared to results based on a traditional cylindrical reference frame. Qualitative indication of general streamfield characteristics as well as quantitative benchmarks for the planning of future experimentation are provided. In addition, preliminary results of an augmented k-ε turbulence model analysis, which explicitly accounts for the effects of streamline curvature and pressure strain in internal turbulent flows, are presented. Specific model difficulties are discussed and comparisons with standard k-ε model predictions are included.

17. KEY WORDS	18. DISTRIBUTION STATEMENT
Turbulence Fluid Dynamics Computational Fluid Dynamics Turbulent Mixing Curvature	Unclassified-Unlimited Subject Category 02

19. SECURITY CLASSIF. (of this report)	20. SECURITY CLASSIF. (of this page)	21. NO. OF PAGES	22. PRICE
Unclassified	Unclassified	32	A03

For sale by National Technical Information Service, Springfield, Virginia 22161
NASA-Langley, 1986